Inversion-symmetric electron gases as platforms for topological planar Josephson junctions

Jiong Mei,[1,2] Kun Jiang,[1,2] Shengshan Qin,[3,*] and Jiangping Hu[1,4,5,†]

[1]*Beijing National Laboratory for Condensed Matter Physics and Institute of Physics, Chinese Academy of Sciences, Beijing 100190, China*

[2]*School of Physical Sciences, University of Chinese Academy of Sciences, Beijing 100190, China*

[3]*School of Physics, Beijing Institute of Technology, Beijing 100081, China*

[4]*Kavli Institute for Theoretical Sciences and CAS Center for Excellence in Topological Quantum Computation, University of Chinese Academy of Sciences, Beijing 100190, China*

[5]*New Cornerstone Science Laboratory, Beijing 100190, China*

(Received 17 March 2024; revised 16 August 2024; accepted 20 August 2024; published 3 September 2024)

Intrinsic Rashba spin-orbital coupling (SOC) can exist in centrosymmetric materials with local inversion symmetry breaking. Here we show that such a SOC can induce topological superconductivity together with an in-plane Zeeman field in planar Josephson junctions formed by the centrosymmetric materials. A single Majorana mode can be created at each end of the junction. We demonstrate this result in a model respecting the same symmetry group with the iron-based superconductors. We derive the necessary Fermi surface condition for the topological planar junction and calculate the topological phase diagram with respect to the in-plane Zeeman field and the phase difference between the two superconductors. We provide experimental characteristics for the topological superconductivity, including the differential conductance and the Fano factor tomography which can be measured in the scanning tunneling spectroscopy. Our study reveals that the centrosymmetric systems with local-inversion-symmetry breaking can serve as new platforms for the topological planar Josephson junctions and helps to find more experimentally feasible materials for the topological superconductors.

DOI: 10.1103/PhysRevB.110.104503

I. INTRODUCTION

Majorana mode is a special kind of quasiparticle whose antiparticle is the particle itself and it usually appears at the topological defects or on the edges of topological superconductors [1–6]. The search for the Majorana modes is not only of fundamental scientific significance, but also of great importance for the realization of fault-tolerant quantum computing [7,8]. Over the past decades, tremendous effort has been made in the study of the topological superconductors [9–41] and great progress has been achieved [42–57], especially in the artificial superconducting heterostructures [43–48,56]. One famous proposal for the topological superconductivity is the Fu-Kane proposal [9]. It is found that, in proximity with conventional superconductors, the superconducting surface Dirac cone of a three-dimensional (3D) strong topological insulator becomes a topological superconductor and a single Majorana zero-energy mode (MZM) is expected in each vortex on the surface. In experiments, the superconducting surface Dirac cone has been verified in $Bi_2Se_3/NbSe_2$ [46], $Bi_2Te_3/NbSe_2$ [47], and in some iron-based superconductors [49], and evidences for the vortex bound MZMs have been detected [48,50–54,57]. Many other superconducting heterostructures have also been proposed to realize the topological superconductivity and signatures for the MZMs have been observed experimentally, such as the 1D Rashba nanowires proximity to conventional superconductors [11,12,44], magnetic atomic chain deposited on superconductors [17–20,45], etc.

Josephson junctions are another promising artificial heterostructure to realize the topological superconductivity and the MZMs [9,58–71]. Recently, the planar Josephson junction constructed by a 2D electron gas with strong spin-orbit coupling and a conventional superconductor has been suggested to be a platform for engineering topological superconductivity [62,63]; with an external magnetic field, the planar junction can host topological superconductivity. Interestingly, in such a topological junction the MZMs can be conveniently controlled by the superconducting phase and in the π-junction condition even a rather small magnetic field can drive the system into the topologically nontrivial state. Moreover, a setup based on the topological Josephson junctions can be convenient to realize topological superconductor networks implementing the non-Abelian braiding [63,64]. In recent experiments, signatures for the existence of the MZMs in the planar Josephson junctions have been observed [65,66].

However, for a long time, the construction of topological junctions has been limited to noncentrosymmetric Rashba electron gases and the exploration of centrosymmetric materials has been lacking, which actually hinders the pursuit of MZMs. In this work, we validate the centrosymmetric systems as material candidates for the topological planar Josephson junctions. We focus on materials with local-inversion-symmetry-breaking crystal structures [72], which are globally centrosymmetric but allow intrinsic Rashba spin-orbit coupling, and demonstrate that such centrosymmetric materials can serve as new platforms for the topological planar Josephson junctions.

*Contact author: qinshengshan@bit.edu.cn

†Contact author: jphu@iphy.ac.cn

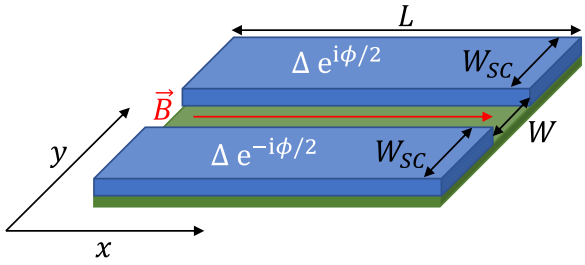

FIG. 1. Setup of a topological planar Josephson junction. In the work, we consider a 2D centrosymmetric electron gas (green) is in proximity with two separate conventional superconductors with a phase difference ϕ. An in-plane magnetic field $\vec{B}$ is applied parallel to the junction.

II. MODEL

We first use a simple model to demonstrate the above assertion. We consider the planar Josephson junction sketched in Fig. 1, which is composed with an electron gas and two superconductor leads. Typically, we are interested in the case in which the aspect ratio of the junction is large ($L, W_{SC} \gg W$). It has been shown that such Josephson junctions are promising to realize topological superconductivity, when the electron gas has strong Rashba spin-orbit coupling stemming from the absence of inversion symmetry [62,63]. Different from the previous studies, in our consideration we focus on the inversion-symmetric electron gas. Specifically, we consider the electron gas in materials with local-inversion-symmetry-breaking crystal structures. One key feature for such materials is that, though they are globally inversion symmetric, the materials can have strong Rashba spin-orbit coupling due to the intrinsic electric dipole arising from the special crystal structures [72–74]. Therefore, we expect such centrosymmetric materials share some similarities with the noncentrosymmetric ones. In the specific model, we consider an electron gas respecting similar crystal structures with the iron-based superconductors, which is a typical structure with local-inversion-symmetry breaking, and the Hamiltonian reads as [74,75]

$$H_0(\boldsymbol{k}) = 2t(\cos k_x + \cos k_y)\sigma_0 s_0 + 2R \sin k_x \sigma_3 s_2 + 2R \sin k_y \sigma_3 s_1 + 4t_1 \cos\frac{k_x}{2}\cos\frac{k_y}{2}\sigma_1 s_0, \quad (1)$$

where s, σ are Pauli matrices representing the spin and sublattice degrees of freedom, respectively. Actually, the Hamiltonian in Eq. (1) describes a situation where an s orbital is put on each iron lattice site in the monolayer FeSe respecting the space group $P4/nmm$. In the model, t is the nearest-neighborhood (NN) intrasublattice hopping, t_1 is the NN intersublattice hopping, and R is the NN intrasublattice Rashba spin-orbit coupling which maintains the inversion symmetry. Here, we note that different from the single-band Rashba electron gas considered in Ref. [62] which lacks the inversion symmetry, the system in our consideration in Eq. (1) is inversion symmetric. The inversion symmetry operator takes the form $\hat{I}_P = \sigma_1 s_0$, since the spin is preserved but the two sublattices are exchanged under the inversion symmetry in our model [74] and it can be straightforwardly checked that the model Hamiltonian satisfies $\hat{I}_P H_0(\boldsymbol{k})\hat{I}_P^{-1} = H_0(-\boldsymbol{k})$. Moreover, the bands depicted by $H_0(\boldsymbol{k})$ are doubly degenerate at every point in the Brillouin zone due to the inversion symmetry and the time reversal symmetry existing simultaneously. It is worth mentioning that the symmetry group of the crystal enforces fourfold band degeneracy at the time reversal invariant points except $(0, 0)$ in the Brillouin zone, leading to the fact that the Fermi surfaces around these points always come in pairs [76–78]. In the following, we choose the parameters in Eq. (1) as $t = -1$, $t_1 = 0.7$, and $R = 0.6$, and set the chemical potential $\mu = -2.2$ to make the electron gas merely have one twofold degenerate Fermi surface surrounding $(0, 0)$.

The two superconductor leads provide conventional superconductivity for the above electron gas through the proximity effect and the superconductivity in the two leads have a phase difference ϕ which can be feasibly controlled by an external magnetic flux, as illustrated in Fig. 1. Accordingly, the superconductivity in the electron gas can be depicted by the following Hamiltonian:

$$H_{SC} = \Delta(\boldsymbol{r})\tau_+\sigma_0 s_0 + \Delta^*(\boldsymbol{r})\tau_-\sigma_0 s_0, \quad (2)$$

where τ is the Pauli matrix in the Nambu space with $\tau_\pm = (\tau_1 \pm i\tau_2)/2$ and the Hamiltonian is written in the basis $(\psi_{\boldsymbol{k}}, is_2\psi^\dagger_{-\boldsymbol{k}})$ with $\psi_{\boldsymbol{k}}$ being the basis of $H_0(\boldsymbol{k})$ in Eq. (1). In Eq. (2), $\Delta(\boldsymbol{r}) = \Delta e^{i\,\mathrm{sgn}(y)\phi/2}\Theta(|y| - W/2)$, where sgn() is the sign function, $\Theta()$ the step function, and W the width of the junction as shown in Fig. 1.

We also consider an in-plane magnetic field applied parallel to the junction as illustrated in Fig. 1, leading to a Zeeman splitting in the electron gas which can be described as

$$H_Z = E_Z(y)\sigma_0 s_1. \quad (3)$$

In the above equation, the Zeeman energy takes the form $E_Z(y) = g(y)\mu_B B/2$, with B being the strength of the magnetic field, $g(y)$ the Landé factor, and μ_B the Bohr magneton. In general, the g factors can be different for that in the junction and that underneath the superconductor leads. Therefore, the Zeeman energy of the electron gas takes the form $E_Z(y) = E_{Z,L}\theta(|y| - W/2) + E_{Z,J}\theta(W/2 - |y|)$. In the following, for simplicity we assume a zero Zeeman energy for electron underneath the leads and discuss the nonzero $E_{Z,L}$ case in the Supplemental Material [79].

III. TOPOLOGICAL SUPERCONDUCTIVITY

In the planar Josephson junction in Fig. 1, Andreev reflection occurs at the interface between the normal region and the superconducting region and bound states develop in the junction region, i.e., the intermediate region between the two superconductor leads. These Andreev bound states form a quasi-1D system along the junction and we can consider the topological property of the system. Moreover, the in-plane magnetic field and the phase difference between the superconductor leads break the time reversal symmetry of the Josephson junction. Therefore, the quasi-1D system belongs to class D according to the Altland-Zirnbauer classification whose topological property is characterized by a $\mathbb{Z}_2$ topological index [80,81] and in the topologically nontrivial condition one single MZM exists at each end of the junction.

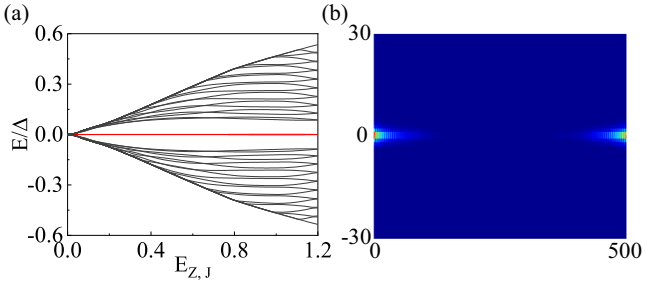

FIG. 2. (a) Quasiparticle energy spectrum for the planar Josephson junction in Fig. 1 with open boundary conditions in both the x and y directions, where the red lines represent the energy of the two Majorana end states. (b) The wave function profiles for the zero energy modes in (a) at $E_Z = 0.4$. The parameters are chosen as $t = -1$, $t_1 = 0.7$, $R = 0.6$, $\phi = \pi$, $\Delta = 0.3$, and the chemical potential is $\mu = -2.2$. In the calculation, we set $W = 2$, $N_x = 500$, and $N_y = 64$.

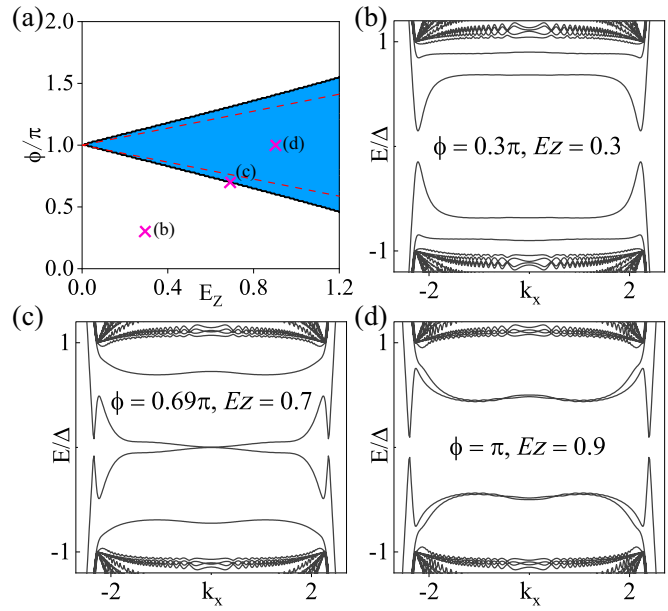

FIG. 3. (a) Topological phase diagram of the planar Josephson junction with respect to the phase difference ϕ and the magnetic field $\vec{B}$ with the blue (white) region representing the topologically nontrivial (trivial) region. The red dashed line is the phase boundary obtained by the analytical formula in Eq. (7). (b)–(d) The superconducting energy spectrum corresponding to the three points marked in the phase diagram in (a). In the calculations, the parameters are chosen as $t = -1$, $t_1 = 0.7$, $R = 0.6$, $\mu = -2.2$, $\Delta = 0.3$, $W = 2$, and $N_y = 64$.

To demonstrate the topological superconductivity in the Josephson junction, we solve the system straightforwardly in the finite condition, i.e., open boundary conditions in both the x and y directions in Fig. 1. By diagonalizing the whole BdG Hamiltonian numerically, we obtain the quasiparticle energy spectrum and find a pair of zero-energy modes with each located at each end of the junction, as shown in Fig. 2. Obviously, the zero-energy modes are the expected MZMs, which is a direct evidence for the topological superconductivity.

It is worth mentioning that in the calculations we find that the topological property of the junction strongly depends on the normal-state Fermi surface condition of the electron gas and the topological superconductivity exists only when the number of Fermi surfaces is odd. Here, when we count the number of the Fermi surfaces, we do not include the double degeneracy caused by the inversion and time reversal symmetries and more details are presented in the Supplemental Material [79].

IV. PHASE DIAGRAM

We calculate the phase diagram for the topological superconductivity in the planar Josephson junction with respect to the phase difference ϕ and the magnetic field $\vec{B}$. As mentioned, the Andreev bound states in the junction form a quasi-1D system which belongs to class D according to the Altland-Zirnbauer classification [80,81]. The topological property of such a system is characterized by the $\mathbb{Z}_2$ topological index, which takes the formula $\mathbb{Z}_2 = \mathrm{sgn}(Pf[M(k_x = 0)]Pf[M(k_x = \pi)])$, with $Pf[M]$ standing for the Pfaffian of the matrix M. In the expression, $M(k_x)$ is the matrix of the BdG Hamiltonian of the whole junction in the Majorana representation, which is antisymmetric due to the particle-hole symmetry existing at the time reversal invariant momentum. By calculating the $\mathbb{Z}_2$ topological index, we achieve the phase diagram for the topological superconductivity in Fig. 3(a). As shown, the topological superconducting state occupies a large region in the phase diagram and in the π junction condition a rather weak in-plane magnetic field can drive the junction into the topologically nontrivial phase. We also verify the phase diagram by simulating the superconducting energy spectrum straightforwardly. As presented in Figs. 3(b)–3(d), a gap-close-reopen process is clearly shown corresponding to the path in the parameter space in Fig. 3(a), indicating a topological phase transition at the phase boundary.

The topological superconductivity in the junction can also be analyzed analytically based on the scattering theory. Before carrying out the analysis, we first simplify the problem. According to the formula of the $\mathbb{Z}_2$ topological index, the topological property of the junction is thoroughly determined by the properties of the system at $k_x = 0$ and $k_x = \pi$. Moreover, considering the Fermi surfaces of the electron gas located near $(0, 0)$, we can merely focus on the BdG Hamiltonian of the planar Josephson junction at $k_x = 0$. Namely, we study the gap-close-reopen process of the superconducting energy spectrum at $k_x = 0$. On the other hand, though the electron gas in Eq. (1) is a two-band system (if not counting the double degeneracy), only one band crosses the Fermi energy with the other band far away from the Fermi energy. Therefore, it is reasonable to discard scattering related to the high-energy band and only consider the scattering from the low-energy band. With the above two points taken into consideration, the problem becomes a case similar to the 1D single-band superconductor-metal-superconductor junction, which is greatly simplified.

Such a problem can be conveniently solved in the continuum limit. At the interface between the normal region and the superconducting region, i.e., at $y = \pm W/2$ in Fig. 1, only pure

Andreev reflection occurs with the scattering matrix being

$$s_{A,j}(\pm W/2) = e^{-i\beta}\begin{pmatrix} 0 & e^{\pm i\phi/2} \\ e^{\mp i\phi/2} & 0 \end{pmatrix}. \tag{4}$$

The scattering matrix is written in the basis $(\psi_j^e(\pm k_e), \quad \psi_j^h(\mp k_h))^T$, where e (h) stands for the electron (hole) and $j = 1, 2$ for the states from the two degenerate Fermi surfaces. In Eq. (4), $\beta = \arccos(\frac{E}{\Delta})$, with E being the energy of the Andreev bound states. By solving the system in different regions and the boundary conditions at the interfaces, we can get the following equation:

$$e^{ik_{e,j}W}e^{-i\beta}e^{-i\phi/2}e^{ik_{h,j}(-W)}e^{-i\beta}e^{-i\phi/2} = 1. \tag{5}$$

After some algebra, we arrive at a simple equation satisfied by the Andreev bound states,

$$\arccos\left(\frac{E}{\Delta}\right) = -\frac{\phi}{2} + \frac{\pi}{2}\frac{E \pm E_Z}{E_T} + n\pi, \tag{6}$$

where n is an integer and $E_T = (\pi/2)v_F/W$ is the corresponding Thouless energy with $v_F = -2tk_F - \frac{2R^2k_F}{\sqrt{R^2k_F^2+4t_1^2}}$ and k_F being the Fermi momentum. Based on Eq. (6), we can immediately determine the boundary between the different topological phases by setting $E = 0$, which turns out to be

$$\phi \bmod 2\pi = (1 \pm E_Z/E_T)\pi \bmod 2\pi. \tag{7}$$

We plot the phase boundary in Fig. 3(a) based on the analytical results in Eq. (7), which matches with the numerical results well. More details on the analytical analysis are presented in the Supplemental Material [79] (see also Ref. [82] therein).

In the above analysis, we assume pure Andreev reflection at the interface between the normal region and the superconducting region. In fact, the topological phase diagram maintains qualitatively unchanged with the phase boundary slightly deformed, even if the normal reflection is considered at the interface. Compared with the previous study [62], the topological phase diagram for the junction constructed with centrosymmetric electron gas here is similar to that constructed with the Rashba electron gas, indicating some similarities between systems with local-inversion-symmetry breaking and the noncentrosymmetric systems.

Here, it is worth pointing out that the scattering theory provides an intuitive understanding on the correspondence between the topological superconductivity and the number of the Fermi surfaces of the electron gas. In the weak pairing condition, the scattering within the same Fermi surface dominates other processes and we can approximately deal with the Andreev bound states from different Fermi surfaces separately. Since each Fermi surface contributes to one MZM at the end of the junction as shown in the above analysis, MZMs from different Fermi surfaces hybridize with each other and only in the condition with odd-number Fermi surfaces can the topological superconductivity in the junction survive considering its $\mathbb{Z}_2$ classification.

V. EXPERIMENTAL CHARACTERIZATION

Finally, we present experimental evidence in scanning tunneling spectroscopy, including the measurements of the zero-bias conductance and the Fano factor tomography [83,84]. In the measurements, the coupling between the tip and the junction takes a general form,

$$H_{\text{tunnel}} = \sum_{i,s}[\tilde{t}_i c_{T,s}^\dagger c_{J,i,s} + \text{H.c.}], \tag{8}$$

where $c_{T,s}$ ($c_{J,i,s}$) is the annihilation operator for the spin s electron in the tip (junction) with i standing for lattice site in the junction. Thus the tunneling events are characterized by the energy width $\Gamma = 2\pi\nu_T\sum_i \tilde{t}_i^2$, where ν_T is the density of states in the tip. The bias voltage V between the tip and the junction is taken into account as $\mu_T = \mu + eV$, with μ_T (μ) the chemical potential for the tip (junction). For simplicity, we assume the tunneling takes place merely between the tip and the lattice sites nearest to the tip in the junction in the simulations. Figure 4(a) shows the zero-bias conductance in the scanning tunneling spectroscopy measurements. Apparently, the quantized zero-bias conductance $2e^2/h$ is a clear signal of the MZMs.

The Fano factor tomography is another useful method to distinguish the MBS from the trivial bound states. The spatially resolved Fano factors are defined as

$$F(i, eV) = \frac{S(i, eV)}{2e|I(i, eV)|}, \tag{9}$$

where $I(i, eV)$ is the dc tunneling current when the tip is located above lattice site i in the junction and $S(i, eV)$ is the

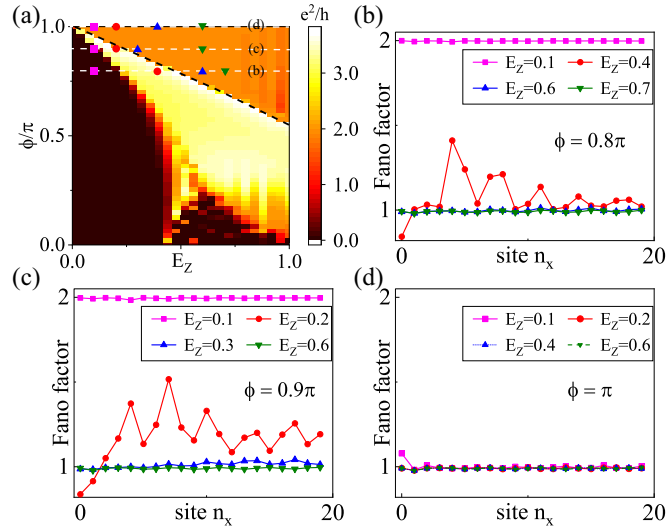

FIG. 4. (a) Zero-bias conductance measured at the end of the junction, where the black dashed line indicates the topological phase boundary. Notice that, in the region near the phase transition boundary, the zero-bias conductance exceeds $2e^2/h$ due to the contributions from the nearly gapless excitations in the junction as indicated in Fig. 3(c). (b)–(d) The spatially resolved Fano factors as the tip moves along the x direction with $n_x = 0$ located at the end of the junction, with respect to different ϕ and E_Z. In the conductance calculations, the energy width is set to $\Gamma = 1.13$ and the temperature is $k_BT = \Delta/8000$, while in the simulations of the Fano factor tomography, we choose $\Gamma = 0.3\Delta$ with a fixed bias voltage $eV_{\text{bias}} = 0.01\Delta$ at the same temperature. The size of the system is set to be $N_x = 800$ and $N_y = 64$. The other parameters of the junction Hamiltonian are the same as those in Fig. 3.

corresponding shot noise. The shot noise is the zero-frequency limit of the time-symmetrized current-current correlator, $S = \int d(t_1 - t_2) S(t_1, t_2)$, where $S(t_1, t_2) = \langle \delta I(t_1) \delta I(t_2) \rangle + \langle \delta I(t_2) \delta I(t_1) \rangle$ and $\delta I(t) = I(t) - \langle I(t) \rangle$. These physical quantities can be calculated through the standard Keldysh formalism [79,83–85]. In the high voltage regime $eV \gg \Gamma_i$, with $\Gamma_i = \Gamma \sum_\sigma (|u_\sigma(i)|^2 + |v_\sigma(i)|^2)$ being the energy width Γ multiplied with the probability of the low lying states at site i, the spatially resolved Fano factors represent the local particle-hole asymmetry of the bound states wave functions [83]. For an isolated MZM which has perfect local particle-hole symmetry, the Fano factor takes a quantized value 1, while for a trivial bound state the spatially resolved Fano factors oscillate between 1 and 2. We calculate the Fano factors at different points in the parameter space (ϕ, E_Z) and present the results in Figs. 4(b)–4(d). As shown, in the topological region a flat plateau $F(n_x) = 1$ is observed in the vicinity of the end of the junction, signaling the existence of the MZM.

VI. DISCUSSION AND CONCLUSION

Recently, the centrosymmetric materials with local-inversion symmetry breaking have been systematically classified and a large number of such kinds of materials have been identified [73,86,87]. As concrete examples, the iron-based superconductors are potential candidates for the construction of the topological planar Josephson junctions. KFe_2As_2 and many 122 families of iron pnictides have three Fermi surfaces at the Brillouin zone center and two Fermi surfaces at the Brillouin zone corner [88–90], which satisfies the requirement of the topological superconductivity in the planar junctions. Besides the iron-based superconductors, the bilayer systems studied in Ref. [91] can also serve as a suitable platform to implement our proposal.

In summary, we show the centrosymmetric materials with local-inversion-symmetry-breaking crystal structures can serve as new material platforms to construct the topological planar Josephson junctions. This result significantly extends material candidates for topological superconductors. Experimental evidence including the differential conductance and the Fano factor tomography in the scanning tunneling spectroscopy measurements are provided to verify the MZMs bound in the junction. Our study can help to find more experimentally feasible materials to realize the long-pursuit MZMs.

ACKNOWLEDGMENTS

This work is supported by the Ministry of Science and Technology (Grant No. 2022YFA1403900), the National Natural Science Foundation of China (Grants No. NSFC-12304163, No. NSFC-11888101, No. NSFC-12174428, and No. NSFC-11920101005), the Strategic Priority Research Program of the Chinese Academy of Sciences (Grants No. XDB28000000 and No. XDB33000000), the New Cornerstone Investigator Program, the Beijing Institute of Technology Research Fund Program for Young Scholars, and the Chinese Academy of Sciences Project for Young Scientists in Basic Research (Grant No. 2022YSBR-048).

[1] X.-L. Qi and S.-C. Zhang, Topological insulators and superconductors, Rev. Mod. Phys. **83**, 1057 (2011).
[2] C.-K. Chiu, J. C. Y. Teo, A. P. Schnyder, and S. Ryu, Classification of topological quantum matter with symmetries, Rev. Mod. Phys. **88**, 035005 (2016).
[3] J. Alicea, New directions in the pursuit of Majorana fermions in solid state systems, Rep. Prog. Phys. **75**, 076501 (2012).
[4] A. Y. Kitaev, Unpaired Majorana fermions in quantum wires, Phys. Usp. **44**, 131 (2001).
[5] N. Read and D. Green, Paired states of fermions in two dimensions with breaking of parity and time-reversal symmetries and the fractional quantum Hall effect, Phys. Rev. B **61**, 10267 (2000).
[6] J. C. Y. Teo and C. L. Kane, Topological defects and gapless modes in insulators and superconductors, Phys. Rev. B **82**, 115120 (2010).
[7] C. Nayak, S. H. Simon, A. Stern, M. Freedman, and S. Das Sarma, Non-abelian anyons and topological quantum computation, Rev. Mod. Phys. **80**, 1083 (2008).
[8] C. Beenakker, Search for Majorana fermions in superconductors, Annu. Rev. Condens. Matter Phys. **4**, 113 (2013).
[9] L. Fu and C. L. Kane, Superconducting proximity effect and Majorana fermions at the surface of a topological insulator, Phys. Rev. Lett. **100**, 096407 (2008).
[10] J. D. Sau, R. M. Lutchyn, S. Tewari, and S. Das Sarma, Generic new platform for topological quantum computation using semiconductor heterostructures, Phys. Rev. Lett. **104**, 040502 (2010).
[11] R. M. Lutchyn, J. D. Sau, and S. Das Sarma, Majorana fermions and a topological phase transition in semiconductor-superconductor heterostructures, Phys. Rev. Lett. **105**, 077001 (2010).
[12] Y. Oreg, G. Refael, and F. von Oppen, Helical liquids and Majorana bound states in quantum wires, Phys. Rev. Lett. **105**, 177002 (2010).
[13] M. Wimmer, A. R. Akhmerov, M. V. Medvedyeva, J. Tworzydło, and C. W. J. Beenakker, Majorana bound states without vortices in topological superconductors with electrostatic defects, Phys. Rev. Lett. **105**, 046803 (2010).
[14] P. Hosur, P. Ghaemi, R. S. K. Mong, and A. Vishwanath, Majorana modes at the ends of superconductor vortices in doped topological insulators, Phys. Rev. Lett. **107**, 097001 (2011).
[15] J. C. Y. Teo and T. L. Hughes, Existence of Majorana-fermion bound states on disclinations and the classification of topological crystalline superconductors in two dimensions, Phys. Rev. Lett. **111**, 047006 (2013).
[16] F. Zhang, C. L. Kane, and E. J. Mele, Time-reversal-invariant topological superconductivity and Majorana Kramers pairs, Phys. Rev. Lett. **111**, 056402 (2013).
[17] F. Pientka, L. I. Glazman, and F. von Oppen, Topological superconducting phase in helical Shiba chains, Phys. Rev. B **88**, 155420 (2013).
[18] S. Nadj-Perge, I. K. Drozdov, B. A. Bernevig, and A. Yazdani, Proposal for realizing Majorana fermions in chains of magnetic atoms on a superconductor, Phys. Rev. B **88**, 020407(R) (2013).

[19] J. D. Sau and P. M. R. Brydon, Bound states of a ferromagnetic wire in a superconductor, Phys. Rev. Lett. **115**, 127003 (2015).

[20] J. Li, T. Neupert, B. A. Bernevig, and A. Yazdani, Manipulating Majorana zero modes on atomic rings with an external magnetic field, Nat. Commun. **7**, 10395 (2016).

[21] G. Xu, B. Lian, P. Tang, X.-L. Qi, and S.-C. Zhang, Topological superconductivity on the surface of Fe-based superconductors, Phys. Rev. Lett. **117**, 047001 (2016).

[22] G. Yang, P. Stano, J. Klinovaja, and D. Loss, Majorana bound states in magnetic skyrmions, Phys. Rev. B **93**, 224505 (2016).

[23] K. Jiang, X. Dai, and Z. Wang, Quantum anomalous vortex and Majorana zero mode in iron-based superconductor Fe(Te,Se), Phys. Rev. X **9**, 011033 (2019).

[24] Y. Ueno, A. Yamakage, Y. Tanaka, and M. Sato, Symmetry-protected Majorana fermions in topological crystalline superconductors: Theory and application to Sr_2RuO_4, Phys. Rev. Lett. **111**, 087002 (2013).

[25] Y. Tsutsumi, M. Ishikawa, T. Kawakami, T. Mizushima, M. Sato, M. Ichioka, and K. Machida, UPt_3 as a topological crystalline superconductor, J. Phys. Soc. Jpn. **82**, 113707 (2013).

[26] F. Zhang, C. L. Kane, and E. J. Mele, Topological mirror superconductivity, Phys. Rev. Lett. **111**, 056403 (2013).

[27] C. Fang, M. J. Gilbert, and B. A. Bernevig, New class of topological superconductors protected by magnetic group symmetries, Phys. Rev. Lett. **112**, 106401 (2014).

[28] S. Kobayashi and M. Sato, Topological superconductivity in Dirac semimetals, Phys. Rev. Lett. **115**, 187001 (2015).

[29] S. Qin, L. Hu, C. Le, J. Zeng, F.-C. Zhang, C. Fang, and J. Hu, Quasi-1D topological nodal vortex line phase in doped superconducting 3D Dirac semimetals, Phys. Rev. Lett. **123**, 027003 (2019).

[30] E. J. König and P. Coleman, Crystalline-symmetry-protected helical Majorana modes in the iron pnictides, Phys. Rev. Lett. **122**, 207001 (2019).

[31] S. Qin, L. Hu, X. Wu, X. Dai, C. Fang, F.-C. Zhang, and J. Hu, Topological vortex phase transitions in iron-based superconductors, Sci. Bull. **64**, 1207 (2019).

[32] R.-X. Zhang, Y.-T. Hsu, and S. Das Sarma, Higher-order topological Dirac superconductors, Phys. Rev. B **102**, 094503 (2020).

[33] Q.-Z. Wang and C.-X. Liu, Topological nonsymmorphic crystalline superconductors, Phys. Rev. B **93**, 020505(R) (2016).

[34] A. Daido, T. Yoshida, and Y. Yanase, $\mathbb{Z}_4$ topological superconductivity in UCoGe, Phys. Rev. Lett. **122**, 227001 (2019).

[35] X.-L. Qi, T. L. Hughes, and S.-C. Zhang, Topological invariants for the fermi surface of a time-reversal-invariant superconductor, Phys. Rev. B **81**, 134508 (2010).

[36] S. Ono, H. C. Po, and H. Watanabe, Refined symmetry indicators for topological superconductors in all space groups, Sci. Adv. **6**, eaaz8367 (2020).

[37] Z. Yan, F. Song, and Z. Wang, Majorana corner modes in a high-temperature platform, Phys. Rev. Lett. **121**, 096803 (2018).

[38] Q. Wang, C.-C. Liu, Y.-M. Lu, and F. Zhang, High-temperature Majorana corner states, Phys. Rev. Lett. **121**, 186801 (2018).

[39] R.-X. Zhang, W. S. Cole, and S. Das Sarma, Helical hinge Majorana modes in iron-based superconductors, Phys. Rev. Lett. **122**, 187001 (2019).

[40] X. Wu, W. A. Benalcazar, Y. Li, R. Thomale, C.-X. Liu, and J. Hu, Boundary-obstructed topological high-T_c superconductivity in iron pnictides, Phys. Rev. X **10**, 041014 (2020).

[41] N. Hao and J. Hu, Topological quantum states of matter in iron-based superconductors: from concept to material realization, Natl. Sci. Rev. **6**, 213 (2019).

[42] S. Sasaki, M. Kriener, K. Segawa, K. Yada, Y. Tanaka, M. Sato, and Y. Ando, Topological superconductivity in $Cu_xBi_2Se_3$, Phys. Rev. Lett. **107**, 217001 (2011).

[43] R. M. Lutchyn, E. P. A. M. Bakkers, L. P. Kouwenhoven, P. Krogstrup, C. M. Marcus, and Y. Oreg, Majorana zero modes in superconductor–semiconductor heterostructures, Nat. Rev. Mater. **3**, 52 (2018).

[44] A. Das, Y. Ronen, Y. Most, Y. Oreg, M. Heiblum, and H. Shtrikman, Zero-bias peaks and splitting in an Al–InAs nanowire topological superconductor as a signature of Majorana fermions, Nat. Phys. **8**, 887 (2012).

[45] S. Nadj-Perge, I. K. Drozdov, J. Li, H. Chen, S. Jeon, J. Seo, A. H. MacDonald, B. A. Bernevig, and A. Yazdani, Observation of Majorana fermions in ferromagnetic atomic chains on a superconductor, Science **346**, 602 (2014).

[46] M.-X. Wang, C. Liu, J.-P. Xu, F. Yang, L. Miao, M.-Y. Yao, C. L. Gao, C. Shen, X. Ma, X. Chen, Z.-A. Xu, Y. Liu, S.-C. Zhang, D. Qian, J.-F. Jia, and Q.-K. Xue, The coexistence of superconductivity and topological order in the Bi_2Se_3 thin films, Science **336**, 52 (2012).

[47] J.-P. Xu, C. Liu, M.-X. Wang, J. Ge, Z.-L. Liu, X. Yang, Y. Chen, Y. Liu, Z.-A. Xu, C.-L. Gao, D. Qian, F.-C. Zhang, and J.-F. Jia, Artificial topological superconductor by the proximity effect, Phys. Rev. Lett. **112**, 217001 (2014).

[48] J.-P. Xu, M.-X. Wang, Z. L. Liu, J.-F. Ge, X. Yang, C. Liu, Z. A. Xu, D. Guan, C. L. Gao, D. Qian, Y. Liu, Q.-H. Wang, F.-C. Zhang, Q.-K. Xue, and J.-F. Jia, Experimental detection of a Majorana mode in the core of a magnetic vortex inside a topological insulator-superconductor $Bi_2Te_3/NbSe_2$ heterostructure, Phys. Rev. Lett. **114**, 017001 (2015).

[49] P. Zhang, K. Yaji, T. Hashimoto, Y. Ota, T. Kondo, K. Okazaki, Z. Wang, J. Wen, G. D. Gu, H. Ding, and S. Shin, Observation of topological superconductivity on the surface of an iron-based superconductor, Science **360**, 182 (2018).

[50] D. Wang, L. Kong, P. Fan, H. Chen, S. Zhu, W. Liu, L. Cao, Y. Sun, S. Du, J. Schneeloch, R. Zhong, G. Gu, L. Fu, H. Ding, and H.-J. Gao, Evidence for Majorana bound states in an iron-based superconductor, Science **362**, 333 (2018).

[51] Q. Liu, C. Chen, T. Zhang, R. Peng, Y.-J. Yan, C.-H.-P. Wen, X. Lou, Y.-L. Huang, J.-P. Tian, X.-L. Dong, G.-W. Wang, W.-C. Bao, Q.-H. Wang, Z.-P. Yin, Z.-X. Zhao, and D.-L. Feng, Robust and clean Majorana zero mode in the vortex core of high-temperature superconductor $(Li_{0.84}Fe_{0.16})$OHFeSe, Phys. Rev. X **8**, 041056 (2018).

[52] L. Kong, S. Zhu, M. Papaj, H. Chen, L. Cao, H. Isobe, Y. Xing, W. Liu, D. Wang, P. Fan, Y. Sun, S. Du, J. Schneeloch, R. Zhong, G. Gu, L. Fu, H.-J. Gao, and H. Ding, Half-integer level shift of vortex bound states in an iron-based superconductor, Nat. Phys. **15**, 1181 (2019).

[53] T. Machida, Y. Sun, S. Pyon, S. Takeda, Y. Kohsaka, T. Hanaguri, T. Sasagawa, and T. Tamegai, Zero-energy vortex bound state in the superconducting topological surface state of Fe(Se,Te), Nat. Mater. **18**, 811 (2019).

[54] L. Kong, L. Cao, S. Zhu, M. Papaj, G. Dai, G. Li, P. Fan, W. Liu, F. Yang, X. Wang, S. Du, C. Jin, L. Fu, H.-J. Gao, and H. Ding, Majorana zero modes in impurity-assisted vortex of LiFeAs superconductor, Nat. Commun. **12**, 4146 (2021).

[55] Z. Wang, J. O. Rodriguez, L. Jiao, S. Howard, M. Graham, G. D. Gu, T. L. Hughes, D. K. Morr, and V. Madhavan, Evidence for dispersing 1d Majorana channels in an iron-based superconductor, Science **367**, 104 (2020).

[56] S. Vaitiekėnas, G. W. Winkler, B. van Heck, T. Karzig, M.-T. Deng, K. Flensberg, L. I. Glazman, C. Nayak, P. Krogstrup, R. M. Lutchyn, and C. M. Marcus, Flux-induced topological superconductivity in full-shell nanowires, Science **367**, eaav3392 (2020).

[57] M. Li, G. Li, L. Cao, X. Zhou, X. Wang, C. Jin, C.-K. Chiu, S. J. Pennycook, Z. Wang, and H.-J. Gao, Ordered and tunable Majorana-zero-mode lattice in naturally strained LiFeAs, Nature (London) **606**, 890 (2022).

[58] K. Flensberg, F. von Oppen, and A. Stern, Engineered platforms for topological superconductivity and Majorana zero modes, Nat. Rev. Mater. **6**, 944 (2021).

[59] C. Schrade, A. A. Zyuzin, J. Klinovaja, and D. Loss, Proximity-induced π Josephson junctions in topological insulators and Kramers pairs of Majorana fermions, Phys. Rev. Lett. **115**, 237001 (2015).

[60] Y. Volpez, D. Loss, and J. Klinovaja, Second-order topological superconductivity in π-junction Rashba layers, Phys. Rev. Lett. **122**, 126402 (2019).

[61] A. Stern and E. Berg, Fractional Josephson vortices and braiding of Majorana zero modes in planar superconductor-semiconductor heterostructures, Phys. Rev. Lett. **122**, 107701 (2019).

[62] F. Pientka, A. Keselman, E. Berg, A. Yacoby, A. Stern, and B. I. Halperin, Topological superconductivity in a planar Josephson junction, Phys. Rev. X **7**, 021032 (2017).

[63] M. Hell, M. Leijnse, and K. Flensberg, Two-dimensional platform for networks of Majorana bound states, Phys. Rev. Lett. **118**, 107701 (2017).

[64] T. Zhou, M. C. Dartiailh, W. Mayer, J. E. Han, A. Matos-Abiague, J. Shabani, and I. Žutić, Phase control of Majorana bound states in a topological X junction, Phys. Rev. Lett. **124**, 137001 (2020).

[65] H. Ren, F. Pientka, S. Hart, A. T. Pierce, M. Kosowsky, L. Lunczer, R. Schlereth, B. Scharf, E. M. Hankiewicz, L. W. Molenkamp, B. I. Halperin, and A. Yacoby, Topological superconductivity in a phase-controlled Josephson junction, Nature (London) **569**, 93 (2019).

[66] A. Fornieri, A. M. Whiticar, F. Setiawan, E. Portolés, A. C. C. Drachmann, A. Keselman, S. Gronin, C. Thomas, T. Wang, R. Kallaher, G. C. Gardner, E. Berg, M. J. Manfra, A. Stern, C. M. Marcus, and F. Nichele, Evidence of topological superconductivity in planar Josephson junctions, Nature (London) **569**, 89 (2019).

[67] J. Cayao, P. San-Jose, A. M. Black-Schaffer, R. Aguado, and E. Prada, Majorana splitting from critical currents in Josephson junctions, Phys. Rev. B **96**, 205425 (2017).

[68] Y. Volpez, D. Loss, and J. Klinovaja, Time-reversal invariant topological superconductivity in planar Josephson bijunction, Phys. Rev. Res. **2**, 023415 (2020).

[69] M. Luethi, K. Laubscher, S. Bosco, D. Loss, and J. Klinovaja, Planar Josephson junctions in germanium: Effect of cubic spin-orbit interaction, Phys. Rev. B **107**, 035435 (2023).

[70] M. Luethi, H. F. Legg, K. Laubscher, D. Loss, and J. Klinovaja, Majorana bound states in germanium Josephson junctions via phase control, Phys. Rev. B **108**, 195406 (2023).

[71] A. Maiellaro, J. Settino, C. Guarcello, F. Romeo, and R. Citro, Hallmarks of orbital-flavored Majorana states in Josephson junctions based on oxide nanochannels, Phys. Rev. B **107**, L201405 (2023).

[72] M. H. Fischer, M. Sigrist, D. F. Agterberg, and Y. Yanase, Superconductivity and local inversion-symmetry breaking, Annu. Rev. Condens. Matter Phys. **14**, 153 (2023).

[73] X. Zhang, Q. Liu, J.-W. Luo, A. J. Freeman, and A. Zunger, Hidden spin polarization in inversion-symmetric bulk crystals, Nat. Phys. **10**, 387 (2014).

[74] S. Qin, C. Fang, F.-C. Zhang, and J. Hu, Topological superconductivity in an extended *s*-wave superconductor and its implication to iron-based superconductors, Phys. Rev. X **12**, 011030 (2022).

[75] D. F. Agterberg, T. Shishidou, J. O'Halloran, P. M. R. Brydon, and M. Weinert, Resilient nodeless *d*-wave superconductivity in monolayer fese, Phys. Rev. Lett. **119**, 267001 (2017).

[76] V. Cvetkovic and O. Vafek, Space group symmetry, spin-orbit coupling, and the low-energy effective Hamiltonian for iron-based superconductors, Phys. Rev. B **88**, 134510 (2013).

[77] Z. Zhang, Z. Wu, C. Fang, F.-C. Zhang, J. Hu, Y. Wang, and S. Qin, Symmetry-protected topological superconductivity in magnetic metals, arXiv:2208.10225.

[78] S. Qin, C. Fang, F. chun Zhang, and J. Hu, Spin-triplet superconductivity in nonsymmorphic crystals, arXiv:2208.09409.

[79] See Supplemental Material at http://link.aps.org/supplemental/10.1103/PhysRevB.110.104503 for (i) the tight-binding model for the Josephson junction in real space and numerical results of the open boundary spectrum of the junction with different number of Fermi surfaces, (ii) the detailed analytical analysis on the topological phase transition of the junction based on scattering theory, (iii) the setup for the tunneling measurements and formalism of calculating the tunneling current as well as the current noise, and (iv) cases for nonvanishing Zeeman field underneath the superconductor leads.

[80] A. P. Schnyder, S. Ryu, A. Furusaki, and A. W. W. Ludwig, Classification of topological insulators and superconductors in three spatial dimensions, Phys. Rev. B **78**, 195125 (2008).

[81] S. Ryu, A. P. Schnyder, A. Furusaki, and A. W. W. Ludwig, Topological insulators and superconductors: tenfold way and dimensional hierarchy, New J. Phys. **12**, 065010 (2010).

[82] C. W. J. Beenakker, Universal limit of critical-current fluctuations in mesoscopic Josephson junctions, Phys. Rev. Lett. **67**, 3836 (1991).

[83] V. Perrin, M. Civelli, and P. Simon, Identifying Majorana bound states by tunneling shot-noise tomography, Phys. Rev. B **104**, L121406 (2021).

[84] J. Mei, K. Jiang, and J. Hu, Identifying Majorana zero modes in vortex lattices using fano factor tomography, Phys. Rev. B **109**, 064509 (2024).

[85] G. Stefanucci and R. van Leeuwen, *Nonequilibrium Many-Body Theory of Quantum Systems: A Modern Introduction* (Cambridge University Press, Cambridge, UK, 2013).

[86] S.-L. Wu, K. Sumida, K. Miyamoto, K. Taguchi, T. Yoshikawa, A. Kimura, Y. Ueda, M. Arita, M. Nagao, S. Watauchi, I. Tanaka, and T. Okuda, Direct evidence of hidden local spin polarization in a centrosymmetric superconductor $LaO_{0.55}F_{0.45}BiS_2$, Nat. Commun. **8**, 1919 (2017).

[87] Y. Zhang, P. Liu, H. Sun, S. Zhao, H. Xu, and Q. Liu, Symmetry-assisted protection and compensation of hidden spin polarization in centrosymmetric systems, Chin. Phys. Lett. **37**, 087105 (2020).

[88] D. Wu, J. Jia, J. Yang, W. Hong, Y. Shu, T. Miao, H. Yan, H. Rong, P. Ai, X. Zhang, C. Yin, J. Liu, H. Chen, Y. Yang, C. Peng, C. Li, S. Zhang, F. Zhang, F. Yang, Z. Wang *et al.*, Nodal s± pairing symmetry in an iron-based superconductor with only hole pockets, Nat. Phys. **20**, 571 (2024).

[89] G. Derondeau, F. Bisti, M. Kobayashi, J. Braun, H. Ebert, V. A. Rogalev, M. Shi, T. Schmitt, J. Ma, H. Ding, V. N. Strocov, and J. Minár, Fermi surface and effective masses in photoemission response of the $(Ba_{1-x}K_x)Fe_2As_2$ superconductor, Sci. Rep. **7**, 8787 (2017).

[90] Y. Ota, K. Okazaki, Y. Kotani, T. Shimojima, W. Malaeb, S. Watanabe, C.-T. Chen, K. Kihou, C. H. Lee, A. Iyo, H. Eisaki, T. Saito, H. Fukazawa, Y. Kohori, and S. Shin, Evidence for excluding the possibility of *d*-wave superconducting-gap symmetry in Ba-doped KFe_2As_2, Phys. Rev. B **89**, 081103(R) (2014).

[91] S. Nakosai, Y. Tanaka, and N. Nagaosa, Topological superconductivity in bilayer Rashba system, Phys. Rev. Lett. **108**, 147003 (2012).